

# In-situ Polymerized Siloxane Cages for an Interface-Stable Gel Polymer Electrolyte in Lithium-Metal Batteries

Huafeng Cao<sup>1</sup> & Chao Fu<sup>1</sup> & Hankun Zhang<sup>1</sup> & Yueping Wang<sup>1</sup> & Zhenhuan Zhang<sup>1</sup>  
& Yiquan Luo<sup>1</sup> & Dexian Wei<sup>1</sup> & Gui-Chao Kuang<sup>2</sup> & Benhua Wang<sup>1,\*</sup> & Bowei Ju<sup>3,\*</sup> & Xiangzhi Song<sup>1</sup> & Libao Chen<sup>2,\*</sup>

<sup>1</sup>College of Chemistry & Chemical Engineering, Central South University, Changsha 410083, Hunan Province, China.

<sup>2</sup>State Key Laboratory of Powder Metallurgy, Central South University, Changsha 410083, Hunan Province, China.

<sup>3</sup>Changsha Research Institute of Mining and Metallurgy Co., Ltd., Changsha, 410012, P. R. China.

\*Corresponding authors (E-mails: [benhuawang@csu.edu.cn](mailto:benhuawang@csu.edu.cn) (B. W.); [jubw@minmetals.com](mailto:jubw@minmetals.com) (B. J.); [lbchen@csu.edu.cn](mailto:lbchen@csu.edu.cn) (L. C.))

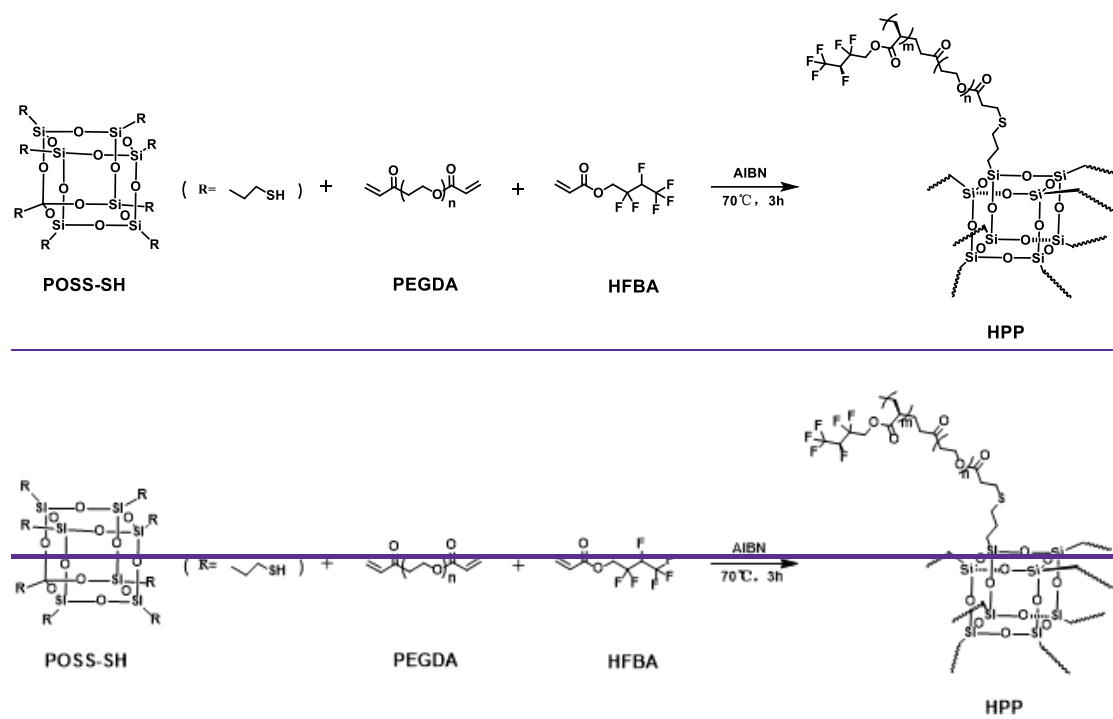


**Figure S1** Schematic diagram of the molecular synthesis strategy for the HPP polymer.

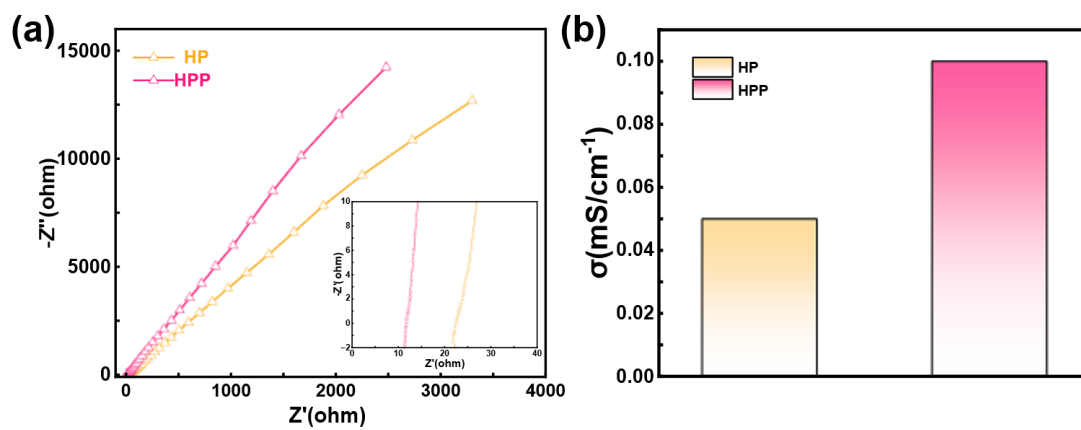


**Figure S2** (a) Impedance spectra measured with blocking electrodes on both sides at room temperature and their magnified views.

(b) Ionic conductivities of HP and HPP polymers calculated from the impedance data.



**Figure S3** Flame retardancy performance diagrams of HPP and HP.

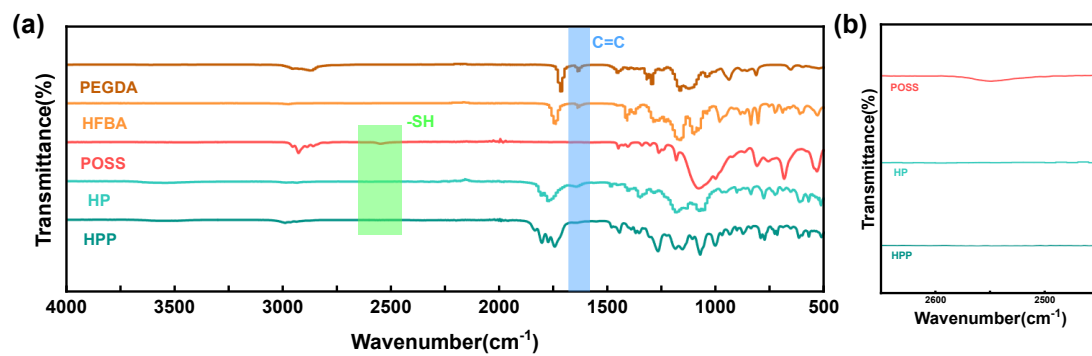


Figure S4 (a) FTIR spectra of polymer precursors and the polymers. (b) Magnified view of the thiol peak.

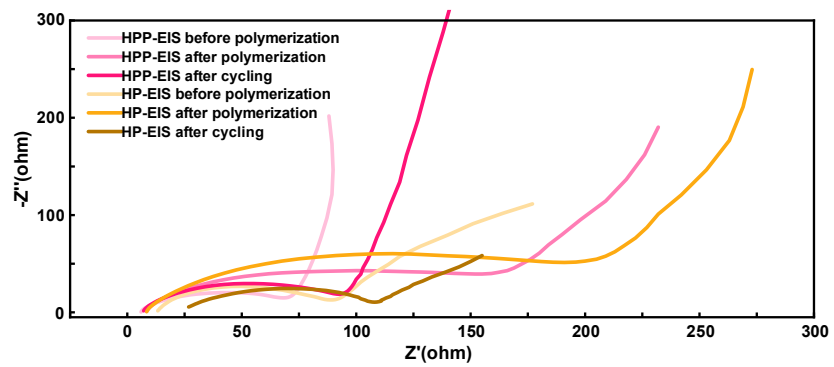
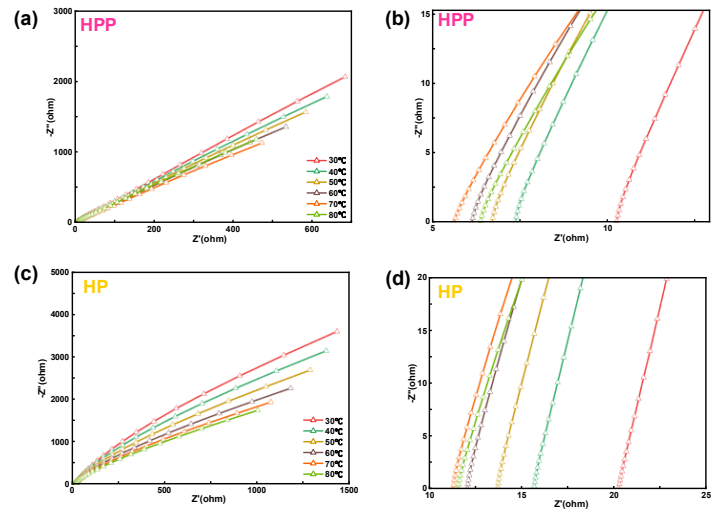
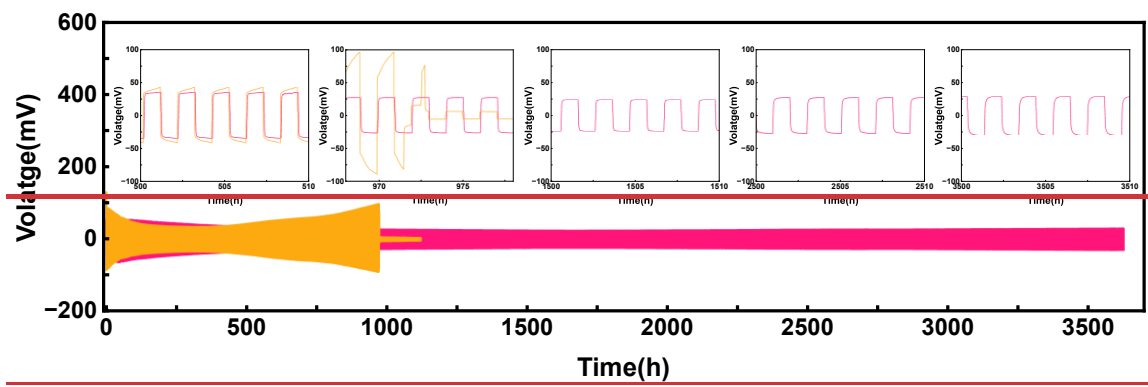
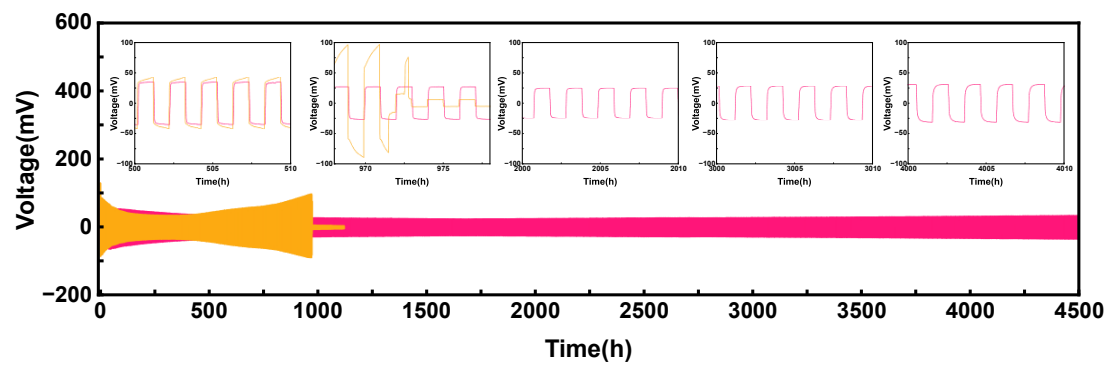


Figure S5 Impedance changes before polymerization, after polymerization, and after 200 cyclescycling.



**Figure S6** Temperature-dependent impedance plots of HPP (a) and HP (c). Magnified views of HPP (b) and HP (d) impedance

plot.



**Figure S7** Long-term cycling performance of Li||Li symmetric cells using HPP and HP. Pink curves represent HPP, and yellow curves represent HP.

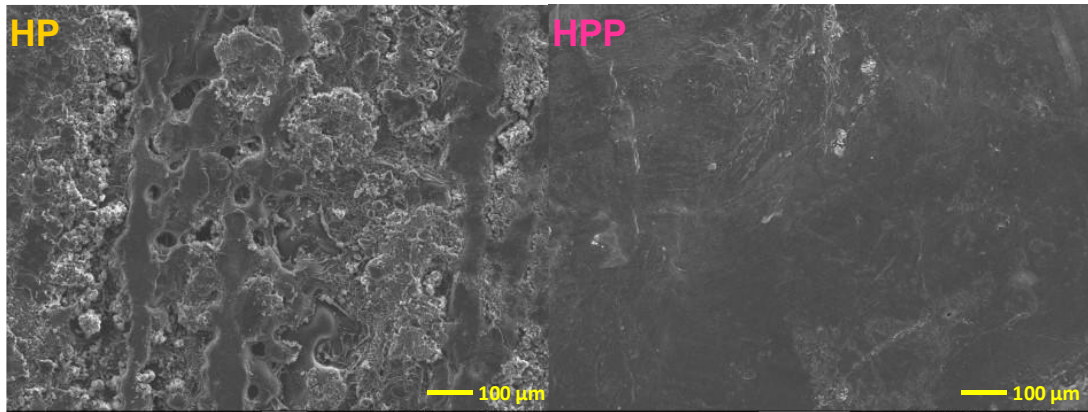


**Figure S8** SEM morphologies of the lithium metal surfaces of HP and HPP at a  $100\ \mu\text{m}$  scale.

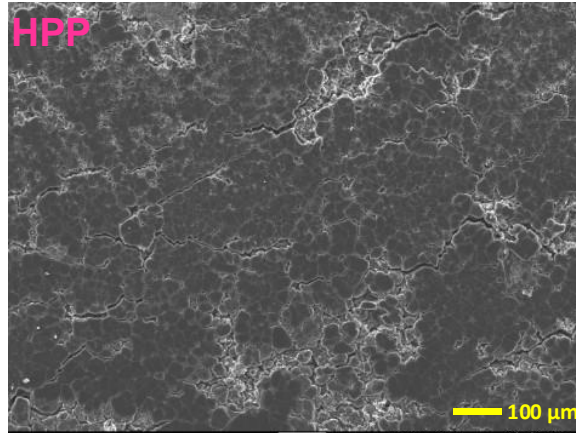


**Figure S9** SEM morphology of the most severely dendritic region on the surface of the HPP lithium metal at a 100  $\mu\text{m}$  scale.

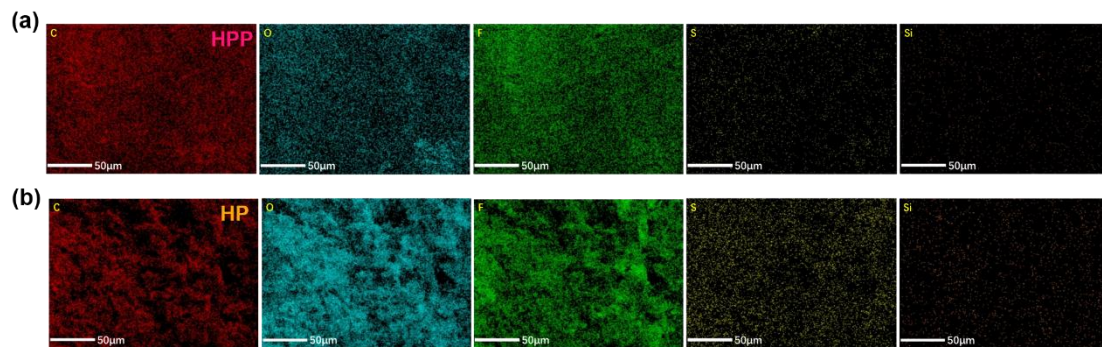


**Figure S10** EDS spectra of C, O, F, S, and Si elements in HPP (a) and HP (b).

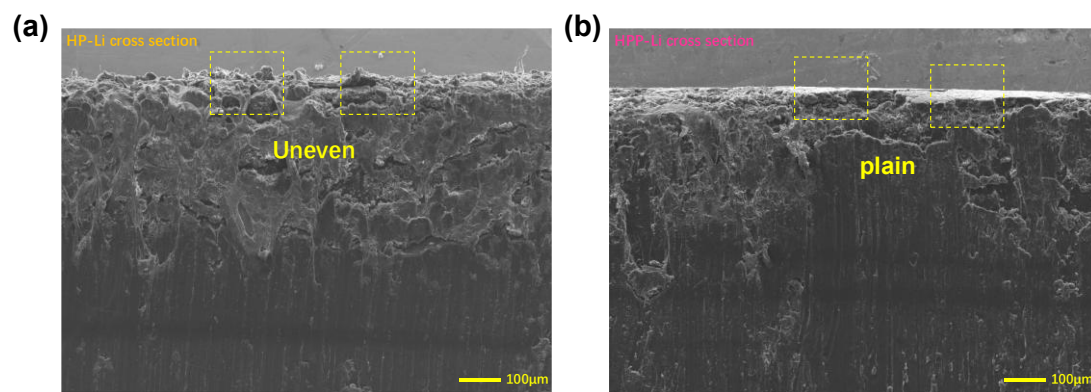


**Figure S11** Cross-sectional SEM images of HP (a) and HPP (b).

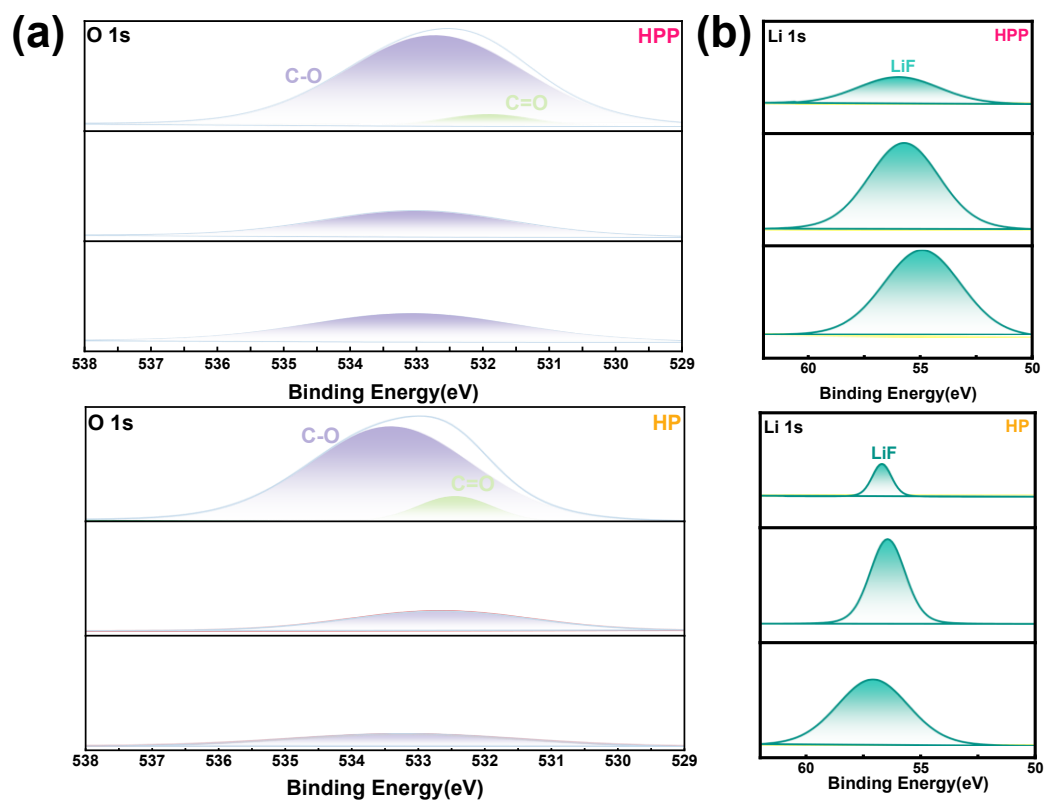


**Figure S12** XPS spectra of O 1s (a) and Li 1s (b) from HPP and HP symmetric cells.

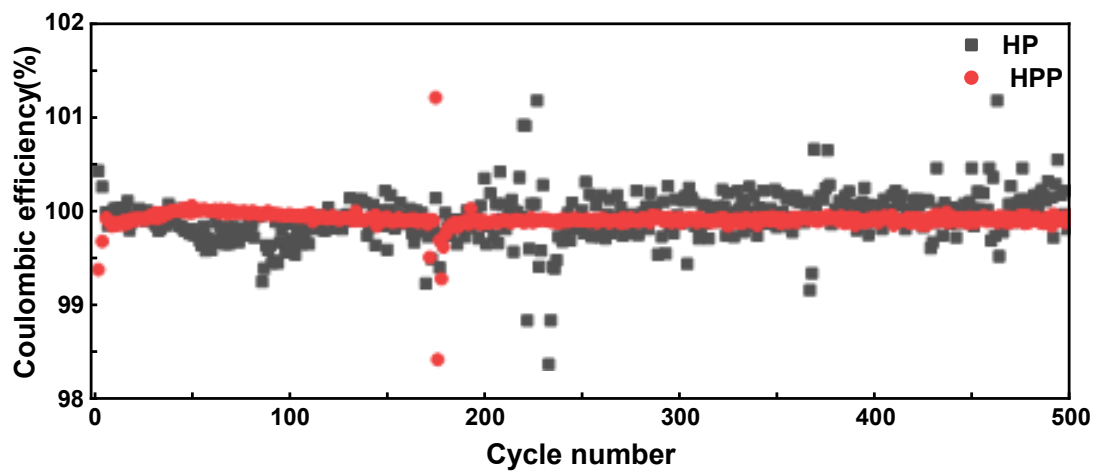


Figure S13 Coulombic efficiency of NCM811 full cells using HP and HPP electrolytes during long-term cycling at a 0.5 C rate.

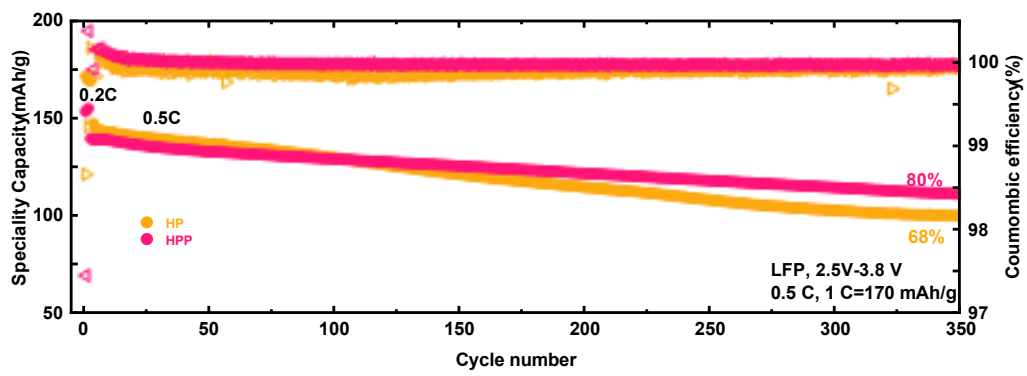
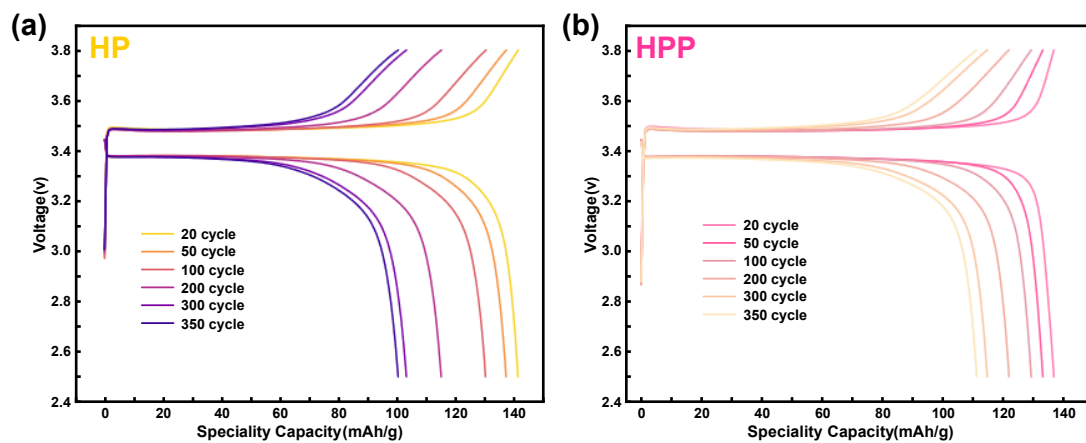
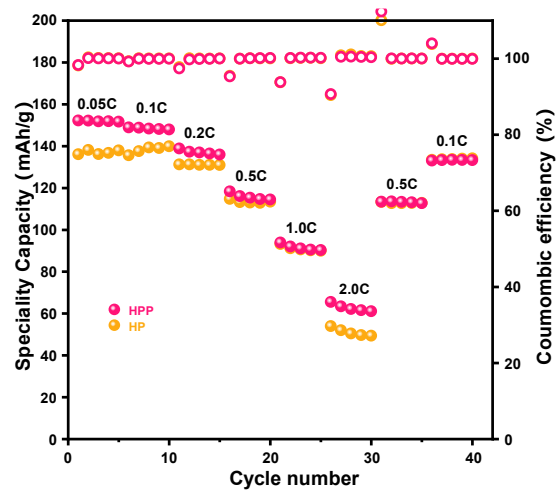


Figure S14 Comparative long-term cycling performance of LFP full cells using HP and HPP electrolytes at a 0.5 C rate.



**Figure S15** Capacity-voltage profiles of long-term cycling performance for LFP full cells using HP (a) and HPP (b) electrolytes

at a 0.5 C rate.



**Figure S16** Rate capability of HP and HPP electrolytes measured in Li||HP||LFP cells.

**Table S1** Summary of Performance for Li||GPE||NCM Batteries

GPE based LMBs	Conductivity of SPE mS cm <sup>-1</sup>	ESW V	Loading mg/cm <sup>-2</sup>	Initial discharge mAh g <sup>-1</sup>	Cutoff voltage V	Capacity retention %	Ref.
Li  HPP  NCM811	0.1@25°C	5.25	2.5	161.59	4.3	79%@500cycles	<i>This work</i>
Li  PFVS  NCM811	0.63@25°C	5.10	2.5	193.2	4.3	81.5%@100cycles	[1]
Li  PBM-IL-Li  NCM811		4.80		115.3	4.3	80%@~50cycles	[2]
Li  HGPE  NCM811	3.4@25°C	5.00	3	199.7	4.5	83.4%@300cycles	[3]
Li  POSS-DOL  NCM811	0.68@25°C	5.00		180.5	4.3	83.5%@400cycles	[4]
Li  NCM83	0.23@-10°C	4.75	2.0	183.2	4.5	85.7%@150cycles	[5]
Li  HSLE  NCM622-TPP	3.03@25°C	3.6	4.5	150	4.3	93%@100cycles	[6]
Li  ALE  NCM622	4.42@-25°C	4.9	6	200	4.3	80%@100cycles	[7]
Li  PHTGPE  NCM811	3.09@25°C	4.59		172.9	4.3	70%@400cycles	[8]
Li  MB-GPE  NCM622	1.95@25°C	5.12	2.5	157	4.3	80.1%@400cycles	[9]
Li  WSGPE    NCM811	0.4@25°C	5.05	1.6	154.8	4.3	92.5% @300cycles	[10]

## References

- [1] Peng H, Long T, Peng J, *et al.* Molecular Design for In-Situ Polymerized Solid Polymer Electrolytes Enabling Stable Cycling of Lithium Metal Batteries. *Adv Energy Mater* 2024; **14**:2400428.
- [2] Wang S, Xiao S, Li S, Organic Cationic-Coordinated Perfluoropolymer Electrolytes with Strong Li<sup>+</sup>-Solvent Interaction for Solid State Li-Metal Batteries. *Angew Chem Int Ed* 2024; **63**: e202412434.
- [3] Wang M, Li M, Wu J, *et al.* Fluoroethylene carbonate-enabled gel polymer electrolyte for stable high-voltage lithium metal batteries. *Adv Mater* 2025; 2502076.
- [4] Xu L, Wang X, Wu Y, *et al.* Ultrastrong nonflammable in-situ polymer electrolyte with enhanced interface stability boosting high-voltage Li metal batteries under harsh conditions. *J Energy Chem* 2025; **102**: 63-72.
- [5] Park J, Seong H, Yuk C, *et al.* Design of fluorinated elastomeric electrolyte for solid-state lithium metal batteries operating at low temperature and high voltage. *Adv Mater* 2024, **36**, 2403191.
- [6] Ma Q, Yue J, Fan M, *et al.* Formulating the electrolyte towards high-energy and safe rechargeable lithium–metal batteries. *Angew Chem Int Ed* 2021; **60**: 16554-16560.
- [7] Jin S, Shan X, Tian J, *et al.* High-entropy gel polymer electrolyte for wide-temperature operatable Li-metal batteries. *Adv Funct Mater* 2025; 2500440.
- [8] Zhou X, Chen Y, Zhen F, *et al.* Dual-Shielding Solvent Strategy of High Dipole-Moment Monomers for Stabilizing Gel Polymer-Based Lithium Metal Batteries. *ACS Nano* 2025; **19**: 14073-14084.
- [9] Zhang S, Li Z, Zhang Y, *et al.* Moderate Li<sup>+</sup> -solvent binding for gel polymer electrolytes with stable cycling toward lithium metal batteries. *Energy Environ Sci* 2025; **18**, 3807-3816.
- [10] Liu S, Tian W, Shen J, *et al.* Bioinspired gel polymer electrolyte for wide temperature lithium metal battery. *Nat Commun* 2025; **16**: 2474.